Computational Statistical Physics

Part I: Statistical Physics and Phase Transitions

Marina Marinkovic

March 9, 2022

ETH Zürich
Institute for Theoretical Physics
HIT G 41.5
Wolfgang-Pauli-Strasse 27
8093 Zürich

402-0812-00L
FS 2022

Monte Carlo Methods – cont.

Creutz Algorithm

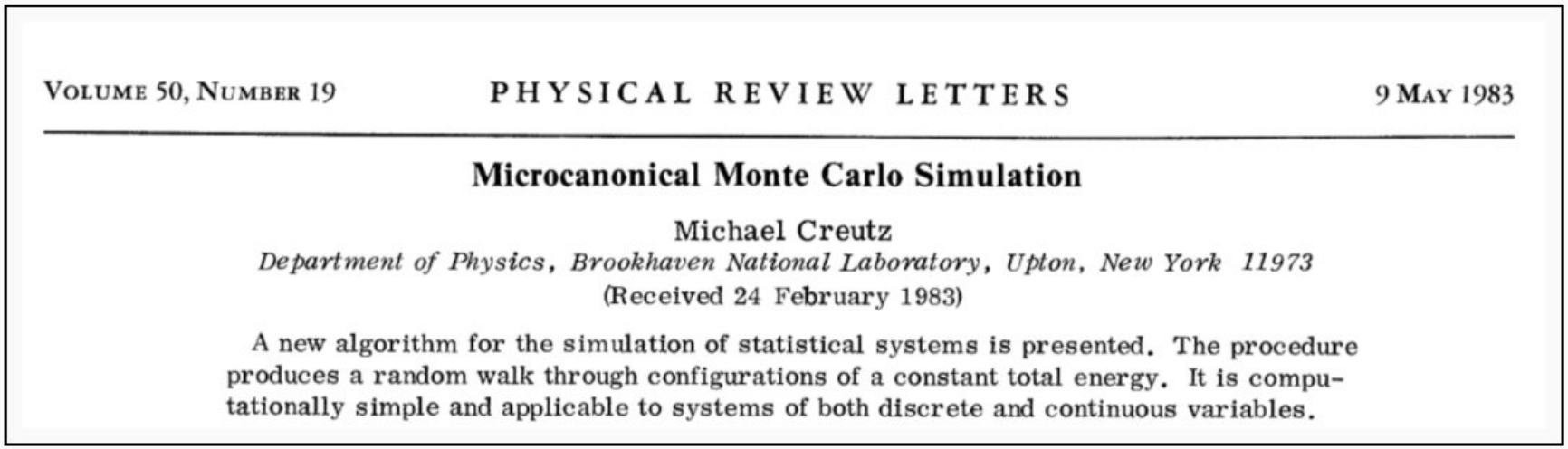

VOLUME 50, NUMBER 19 PHYSICAL REVIEW LETTERS 9 MAY 1983

Microcanonical Monte Carlo Simulation

Michael Creutz
Department of Physics, Brookhaven National Laboratory, Upton, New York 11973
(Received 24 February 1983)

A new algorithm for the simulation of statistical systems is presented. The procedure produces a random walk through configurations of a constant total energy. It is computationally simple and applicable to systems of both discrete and continuous variables.

Figure 1: An algorithm to perform microcanonical Monte Carlo simulations, i.e., system at constant energy.

Creutz Algorithm

The movement in phase space is in fact not strictly constrained to a subspace of constant energy but there is a certain additional volume in which we can freely move. The condition often constant energy is softened by introducing a so-called *demon* which corresponds to a small reservoir of energy E_D that can store a certain maximum energy $E_{\max}$.

Creutz Algorithm

Creutz algorithm

- Choose a site,
- Compute ΔE for the spin flip,
- Accept the change if $E_{\max} \geq E_D - \Delta E \geq 0$.

Pro: Besides the fact that we can randomly choose a site, this method involves no random numbers and is thus said to be completely deterministic and therefore reversible.

Con: The temperature of the system is not known.

Creutz Algorithm

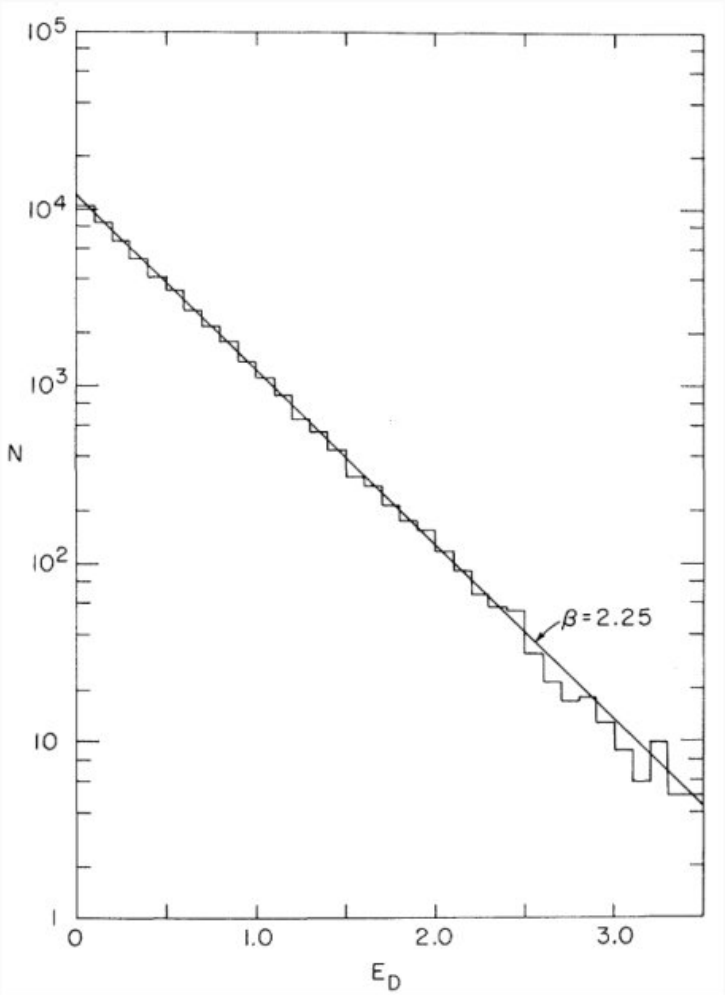

Figure 2: The distribution of the demon energy E_D is exponentially distributed. Based on the Boltzmann factor, it is possible to extract the inverse temperature $\beta = (k_B T)^{-1} = 2.25$. The figure is taken from Ref. shown in Figure 3.

Finite size methods

Finite size methods

Divergent behavior at T_c as described by

$$\chi(T) \sim |T_c - T|^{-\gamma} \tag{1}$$

$$C(T) \sim |T_c - T|^{-\alpha}, \tag{2}$$

$$\xi(T) \sim |T - T_c|^{-\nu} \tag{3}$$

The larger the system size, the more pronounced is the divergence.

Finite size methods

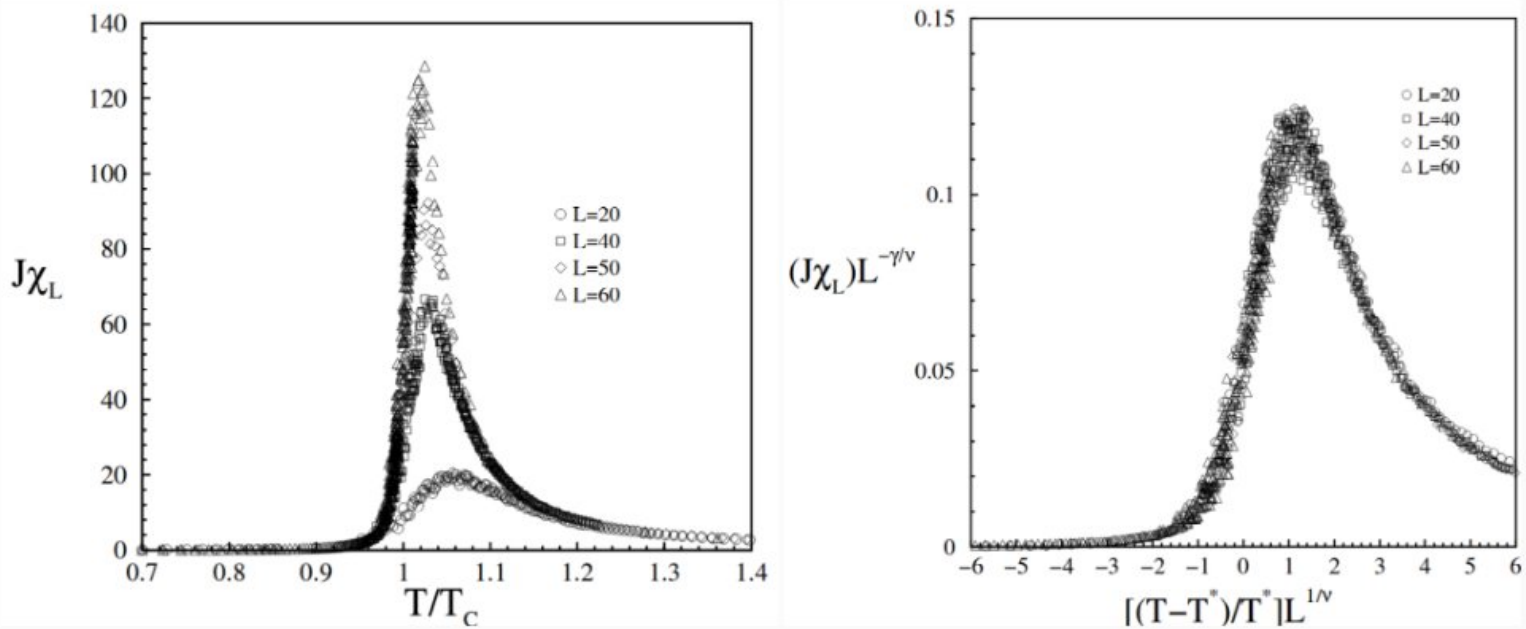

Figure 3: The system size dependence of the susceptibility and the corresponding finite size scaling. The figure is taken from [Da Silva et al., Braz. J. Phys. 32, 2002].

Finite size methods

The finite size scaling relation of the susceptibility is given by

$$\chi\left(T, L\right) = L^{\frac{\gamma}{\nu}} F_{\chi}\left[\left(T - T_c\right) L^{\frac{1}{\nu}}\right], \tag{4}$$

where F_{χ} is called susceptibility *scaling function*[1].

[1] Based on Eq. (1), we can infer that $F_{\chi}\left[\left(T - T_c\right) L^{\frac{1}{\nu}}\right] \sim \left(\left|T - T_c\right| L^{\frac{1}{\nu}}\right)^{-\gamma}$ as $L \to \infty$.

Finite size methods

In the case of the magnetization, the corresponding finite size scaling relation is

$$M_S\left(T, L\right) = L^{-\frac{\beta}{\nu}} F_{M_S}\left[\left(T - T_c\right) L^{\frac{1}{\nu}}\right]. \tag{5}$$

Binder Cumulant

We still need a way to determine T_c more precisely. To tho that, we make use of the so-called *Binder cumulant*

$$U_L = 1 - \frac{\langle M^4 \rangle_L}{3 \langle M^2 \rangle_L^2}, \tag{6}$$

which is independent of the system size L at T_c since

$$\frac{\langle M^4 \rangle_L}{3 \langle M^2 \rangle_L^2} = \frac{L^{-\frac{4\beta}{\nu}} F_{M^4} \left[(T - T_c) L^{\frac{1}{\nu}} \right]}{\left\{ L^{-\frac{2\beta}{\nu}} F_{M^2} \left[(T - T_c) L^{\frac{1}{\nu}} \right] \right\}^2} = F_C \left[(T - T_c) L^{\frac{1}{\nu}} \right]. \tag{7}$$

Binder Cumulant

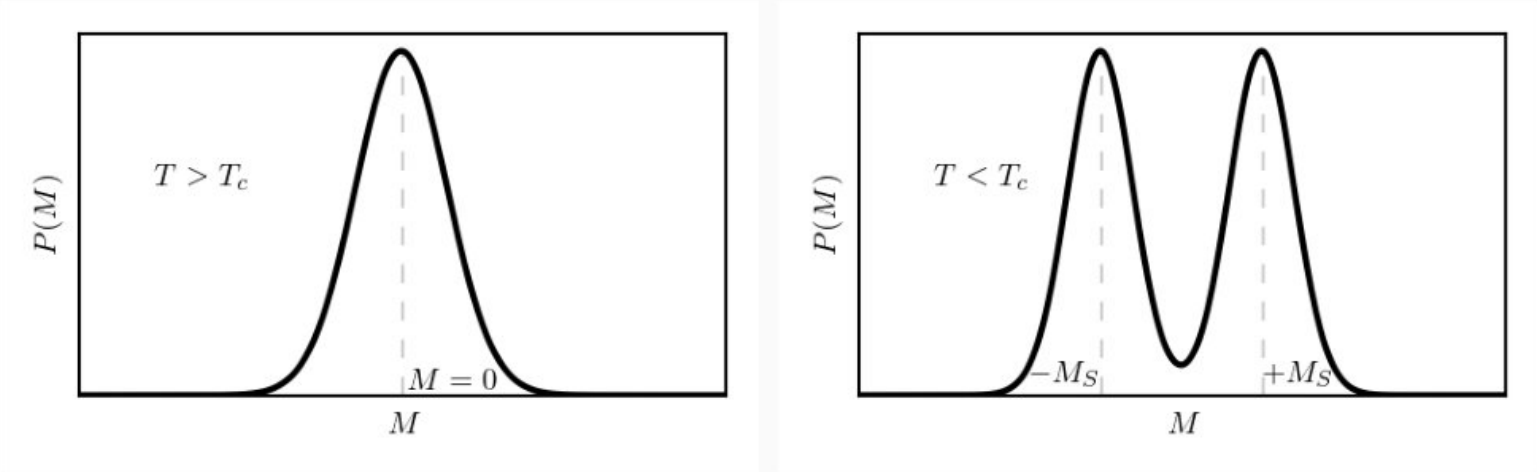

Figure 4: The distribution $P(M)$ of the magnetization M above a below the critical temperature T_c.

Binder Cumulant

For $T > T_c$, the magnetization is described by a Gaussian distribution

$$P_L(M) = \sqrt{\frac{L^d}{\pi\sigma_L}} \exp\left[-\frac{M^2 L^d}{\sigma_L}\right], \tag{8}$$

with $\sigma_L = 2k_B T\chi_L$. Since the fourth moment equals three times the second moment squared, i.e.,

$$\langle M^4 \rangle = 3\langle M^2 \rangle_L^2, \tag{9}$$

it follows that U_L must be zero for $T > T_c$.

Binder Cumulant

Below the critical temperature ($T < T_c$), there exist one ground state with positive and one with negative magnetization and the corresponding distribution is given by

$$P_L(M) = \frac{1}{2}\sqrt{\frac{L^d}{\pi\sigma_l}}\left\{\exp\left[-\frac{(M-M_S)^2 L^d}{\sigma_L}\right] + \exp\left[-\frac{(M+M_S)^2 L^d}{\sigma_L}\right]\right. \tag{10}$$

Binder Cumulant

For this distribution, it holds that $\langle M^4 \rangle = \langle M^2 \rangle_L^2$ and therefore $U_L = \frac{2}{3}$. In summary, we demonstrated that

$$U_L = \begin{cases} \frac{2}{3} & \text{for } T < T_c \\ \text{const} & \text{for } T = T_c \\ 0 & \text{for } T > T_c \end{cases} \tag{11}$$

Binder Cumulant

U_L (T)

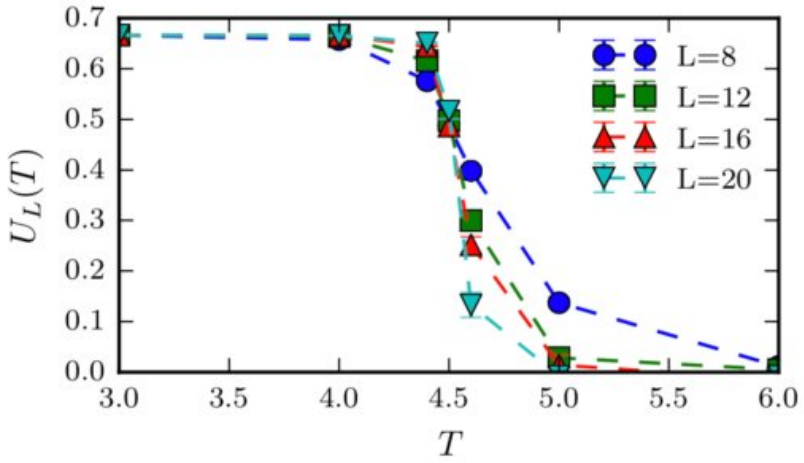

U_L (T) zoomed into [4.49,4.52] temperature region

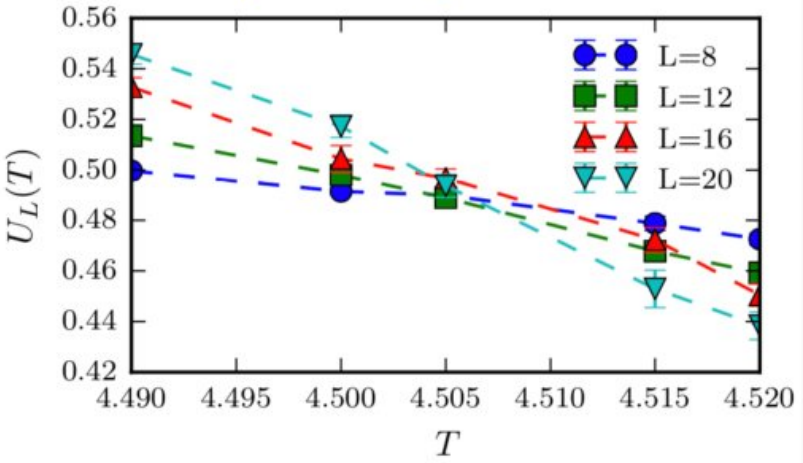

Corrections to Scaling

Far away from T_c we cannot observe a clear power law behavior anymore, and corrections to scaling have to be employed, i.e.,

$$M(T) = A_0 (T_c - T)^{\beta} + A_1 (T_c - T)^{\beta_1} + \ldots, \tag{12}$$

$$\xi(T) = C_0 (T_c - T)^{\nu} + C_1 (T_c - T)^{\nu_1} + \ldots, \tag{13}$$

with $\beta_1 > \beta$ and $\nu_1 < \nu$.

Corrections to Scaling

These corrections are very important for high quality data, where the errors are small and the deviations become visible. The scaling functions must also be generalized as

$$M\left(T,L\right)=L^{-\frac{\beta}{\nu}}F_{M}\left[\left(T-T_{c}\right)L^{\frac{1}{\nu}}\right]+L^{-x}F_{M}^{1}\left[\left(T-T_{c}\right)L^{\frac{1}{\nu}}\right]+\ldots \tag{14}$$

with $x=\max\left[\frac{\beta}{\nu},\frac{\beta}{\nu_{1}},\frac{\beta}{\nu}-1\right]$.

First Order Transition

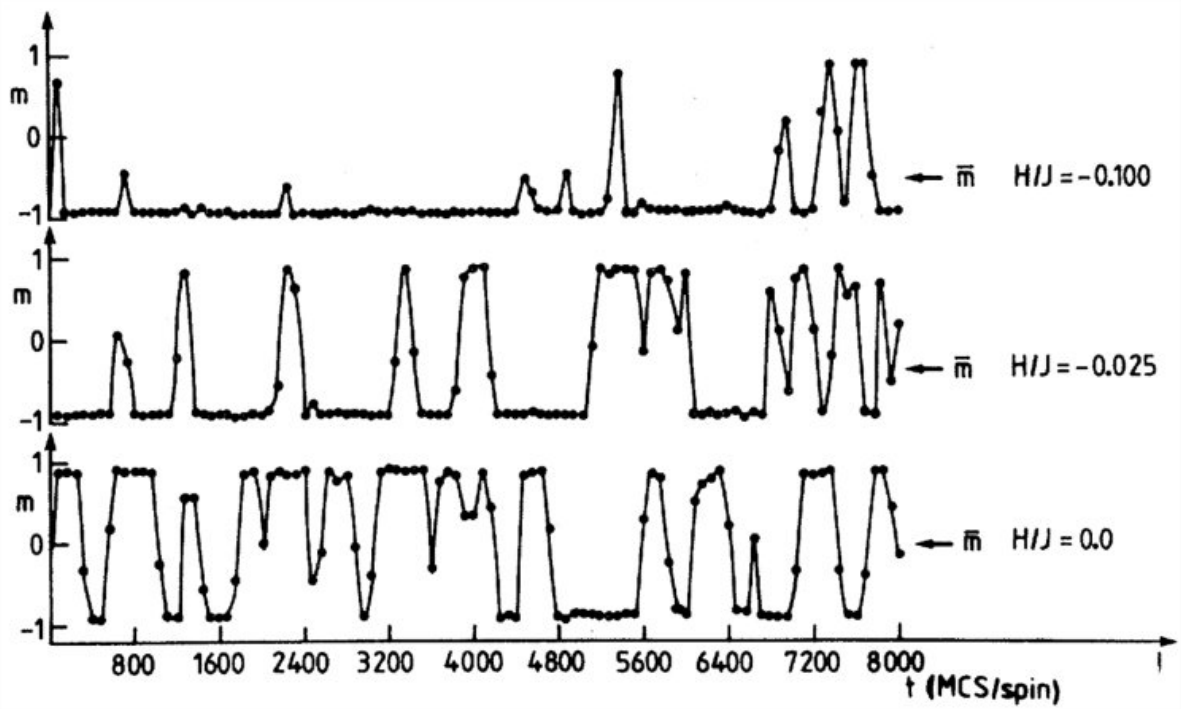

Figure 5: The magnetization exhibits a switching behavior if the field vanishes. For non-zero magnetic fields, the magnetization is driven in the direction of the field. The figure is taken from [Binder and Landau, Phys. Rev. B30 3 (1984)]

First Order Transition

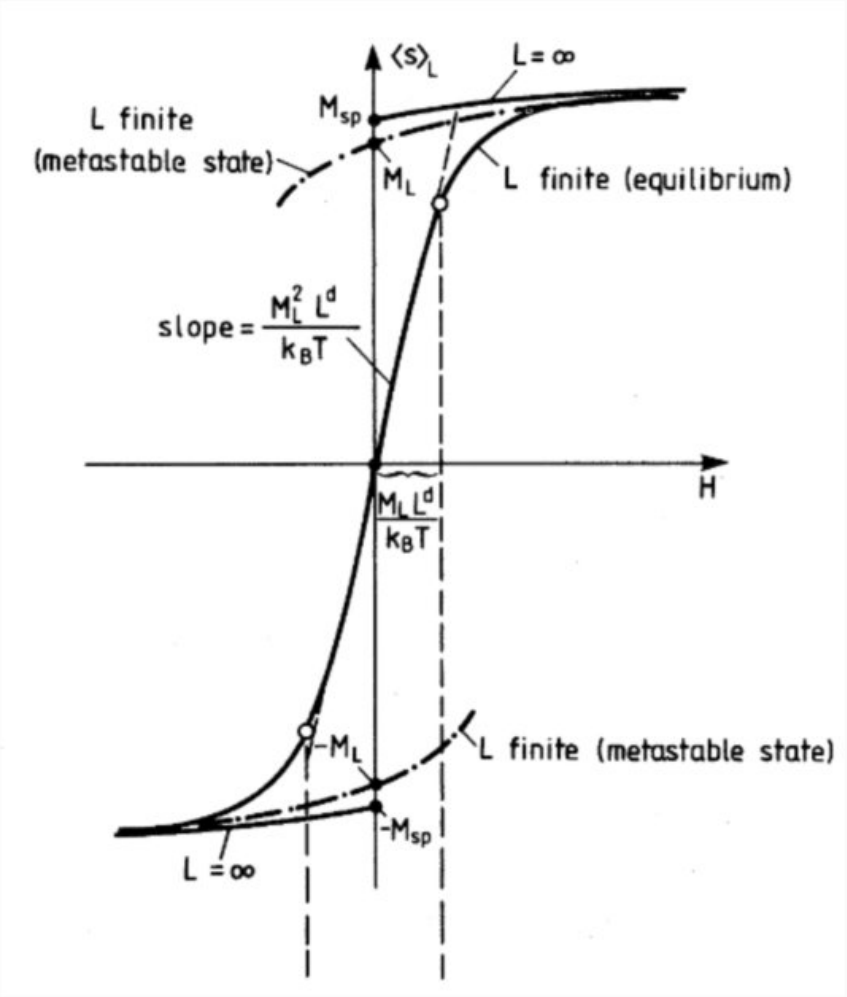

Figure 6: Hysteresis can be found by varying the field from negative to positive values and back. The figure is taken from [Binder and Landau, Phys. Rev. B30 3 (1984)]

First Order Transition

Binder showed that the magnetization as a function of the field H is described by $\tanh\left(\alpha L^d\right)$ if the distribution of the magnetization is given by Eq. (10). Specifically, we find for the magnetization and susceptibility

$$M(H) = \chi_L^D H + M_L \tanh\left(\beta H M_L L^d\right), \tag{15}$$

$$\chi_L(H) = \frac{\partial M}{\partial H} = \chi_L^D + \frac{\beta M_L L^d}{\cosh^2\left(\beta H M_L L^d\right)}. \tag{16}$$

First Order Transition

Similarly, to the scaling of a second order transition, we can scale the maximum of the susceptibility ($\chi_L(H=0) \sim L^d$) and the width of the peak ($\Delta\chi_L \sim L^{-d}$). To summarize, a first order phase transition is characterized by

1. A bimodal distribution of the order parameter,
2. stochastic swichting between the two states in small systems,
3. hysteresis of the order parameter when changing the field,
4. a scaling of the order parameter, or response function according to Eq. (16).

Cluster algorithms

Potts model

The Hamiltonian of the system is defined as

$$\mathcal{H} = -J \sum_{\langle i,j \rangle} \delta_{\sigma_i \sigma_j} - H \sum_i \sigma_i, \tag{17}$$

where $\sigma_i \in \{1, ..., q\}$ and $\delta_{\sigma_i \sigma_j}$ is unity when nodes i and j are in the same state. The Potts model exhibits a first order transition at the critical temperature in two dimensions for $q > 4$, and for $q > 2$ for dimensions larger than two.

Potts model

For $q = 2$, the Potts model is equivalent to the Ising model.

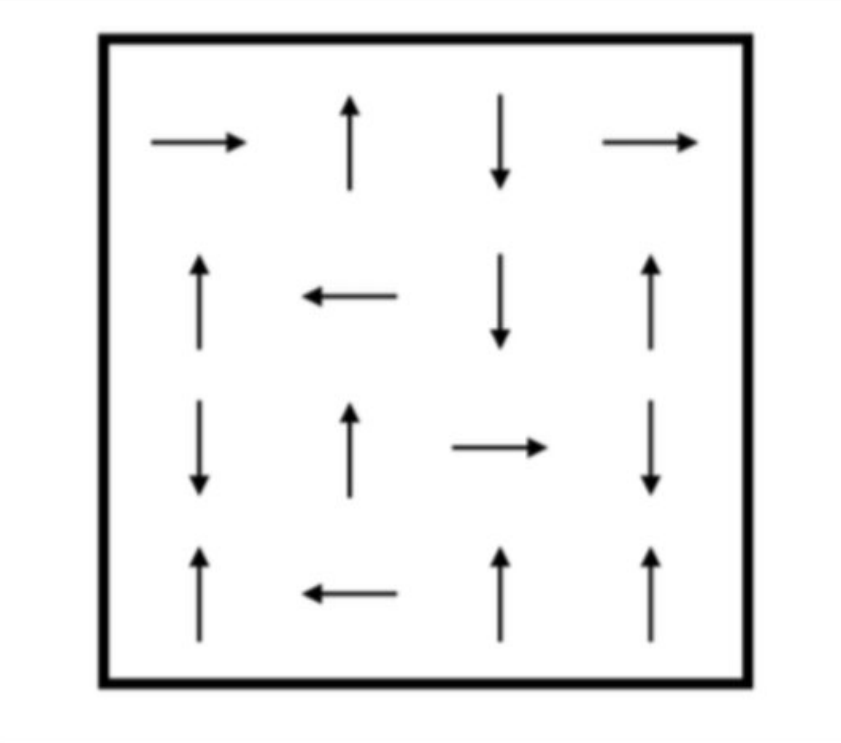

Figure 7: Example of a 4x4 Potts lattice for q=4.

The Kasteleyn and Fortuin Theorem

We consider the Potts model not on a square lattice but on an arbitrary graph of nodes connected with bonds ν. Each node has q possible states and each connection leads to an energy cost of unity if two connected nodes are in a different state and of zero if they are in the same state, i.e.,

$$E = J \sum_{\nu} \epsilon_\nu \quad \text{with} \quad \epsilon_\nu = \begin{cases} 0 & \text{if endpoints are in the same state} \\ 1 & \text{otherwise} \end{cases} \tag{18}$$

The Kasteleyn and Fortuin Theorem

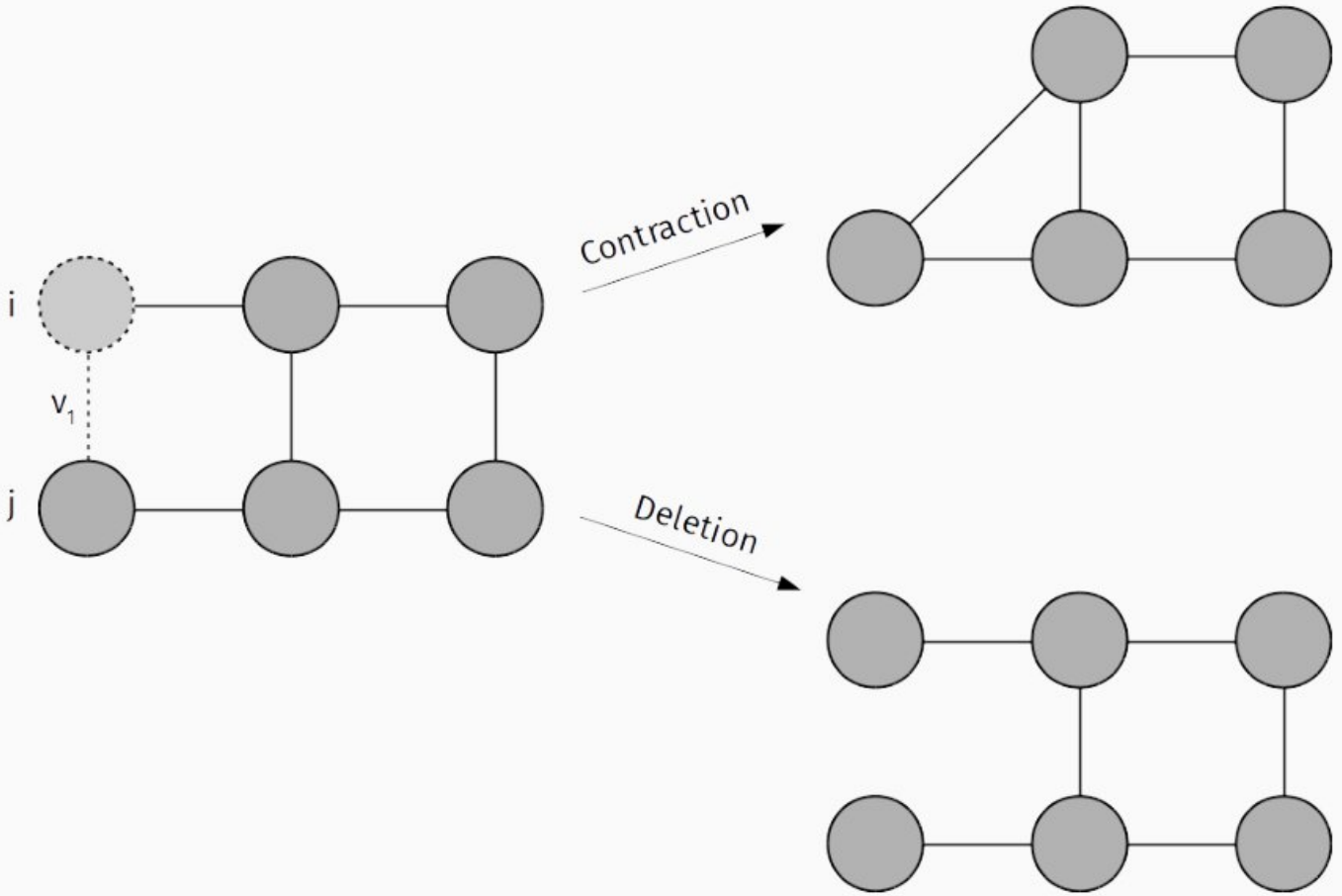

Figure 8: Contraction and deletion on a graph.

The Kasteleyn and Fortuin Theorem

The partition function is the sum over all the possible configurations weighted by the Boltzmann factor and thus given by

$$Z = \sum_X e^{-\beta E(X)} \overset{(18)}{=} \sum_X e^{-\beta J \sum_\nu \epsilon_\nu} = \sum_X \prod_\nu e^{-\beta J \epsilon_\nu}. \qquad (19)$$

The Kasteleyn and Fortuin Theorem

We now consider a graph where bond ν_1 connects two nodes i and j with states σ_i and σ_j, respectively. If we would delete bond ν_1, the partition function is

$$Z_D = \sum_X \prod_{\nu \neq \nu_1} e^{-\beta J \epsilon_\nu}. \tag{20}$$

The Kasteleyn and Fortuin Theorem

We can thus rewrite Eq. (19) as

$$Z = \sum_X e^{-\beta J \epsilon_{\nu_1}} \prod_{\nu \neq \nu_1} e^{-\beta J \epsilon_\nu} = \sum_{X:\sigma_i = \sigma_j} \prod_{\nu \neq \nu_1} e^{-\beta J \epsilon_\nu} + e^{-\beta J} \sum_{X:\sigma_i \neq \sigma_j} \prod_{\nu \neq \nu_1} e^{-}$$

where the first part is the partition function of the contracted graph Z_C and the second part is given by the identity

$$\sum_{X:\sigma_i \neq \sigma_j} \prod_{\nu \neq \nu_1} e^{-\beta J \epsilon_\nu} = \sum_X \prod_{\nu \neq \nu_1} e^{-\beta J \epsilon_\nu} - \sum_{X:\sigma_i = \sigma_j} \prod_{\nu \neq \nu_1} e^{-\beta J \epsilon_\nu} = Z_D - Z_C. \tag{21}$$

The Kasteleyn and Fortuin Theorem

Summarizing the latter results, we find

$$Z = Z_C + e^{-\beta J}\left(Z_D - Z_C\right) = pZ_C + (1-p)Z_D, \qquad (22)$$

where $p = -e^{-\beta J}$. To be more precise, we expressed the partition function Z as the contracted and deleted partition functions at bond ν_1. We apply the latter procedure to another bond ν_2 and find

$$Z = p^2 Z_{C_{\nu_1},C_{\nu_2}} + p(1-p)Z_{C_{\nu_1},D_{\nu_2}} + (1-p)^2 Z_{D_{\nu_1},D_{\nu_2}}. \qquad (23)$$

The Kasteleyn and Fortuin Theorem

After applying these operations to every bond, the graph is reduced to a set of separated points corresponding to clusters of nodes which are connected and in the same state out of q states. The partition function reduces to

$$Z = \sum_{\substack{\text{configurations of} \\ \text{bond percolation}}} q^{\#\text{ of clusters}} p^c (1-p)^d = \left\langle q^{\#\text{ of clusters}} \right\rangle_{\mathsf{b}}, \tag{24}$$

where c and d are the numbers of contracted and deleted bonds respectively. In the limit of $q \to 1$, one obtains the partition function of bond percolation[2].

[2] In bond percolation [Broadbent, Hammersley (1957)], an edge of a graph is occupied with probability p and vacant with probability $1-p$.

Coniglio-Klein clusters

The probability of a given cluster C to be in a certain state σ_0 is independent of the state itself, i.e.,

$$p(C,\sigma_0) = p^{c_C}(1-p)^{d_C} \sum_{\substack{\text{bond percolation} \\ \text{without cluster C}}} q^{\#\text{ of clusters}} p^c\,(1-p)^d. \quad (25)$$

Coniglio-Klein clusters

This implies that flipping this particular cluster has no effect on the partition function (and therefore the energy) so that it is possible to accept the flip with probability one. This can be seen by looking at the detailed balance condition of the system

$$p(C,\sigma_1)W\left[(C,\sigma_1)\to(C,\sigma_2)\right] = p(C,\sigma_2)W\left[(C,\sigma_2)\to(C,\sigma_1)\right] \tag{26}$$

and using $p(C,\sigma_1) = p(C,\sigma_2)$.

Coniglio-Klein clusters

We then obtain for acceptance probabilities

$$W[(C,\sigma_2)\to(C,\sigma_1)] = \frac{p(C,\sigma_2)}{p(C,\sigma_1)+p(C,\sigma_2)} = \frac{1}{2} \quad \text{Glauber dyn} \tag{27}$$

$$W[(C,\sigma_2)\to(C,\sigma_1)] = \min\left[1,\frac{p(C,\sigma_2)}{p(C,\sigma_1)}\right] = 1 \quad \text{Metropolis} \tag{28}$$

Based on these insights, we introduce cluster algorithms which are much faster than single-spin flip algorithms and less prone to the problem of critical slowing down.

Other Ising-like models

One of the possible generalizations of the Ising model is the so called n-vector model. Unlike the Potts model, it describes spins as vectors with n components. This model has applications in modelling magnetism or the Higgs mechanism. The Hamiltonian resembles the one of the Potts model in the sense that it favors spin alignment

$$\mathcal{H} = -J \sum_{\langle i,j \rangle} \vec{S}_i \cdot \vec{S}_j + \vec{H} \sum_i \vec{S}_i. \tag{29}$$

with $\vec{S}_i = \left(S_i^1, S_i^2, \ldots, S_i^n\right)$ and $\left|\vec{S}_i\right| = 1$.

Other Ising-like models

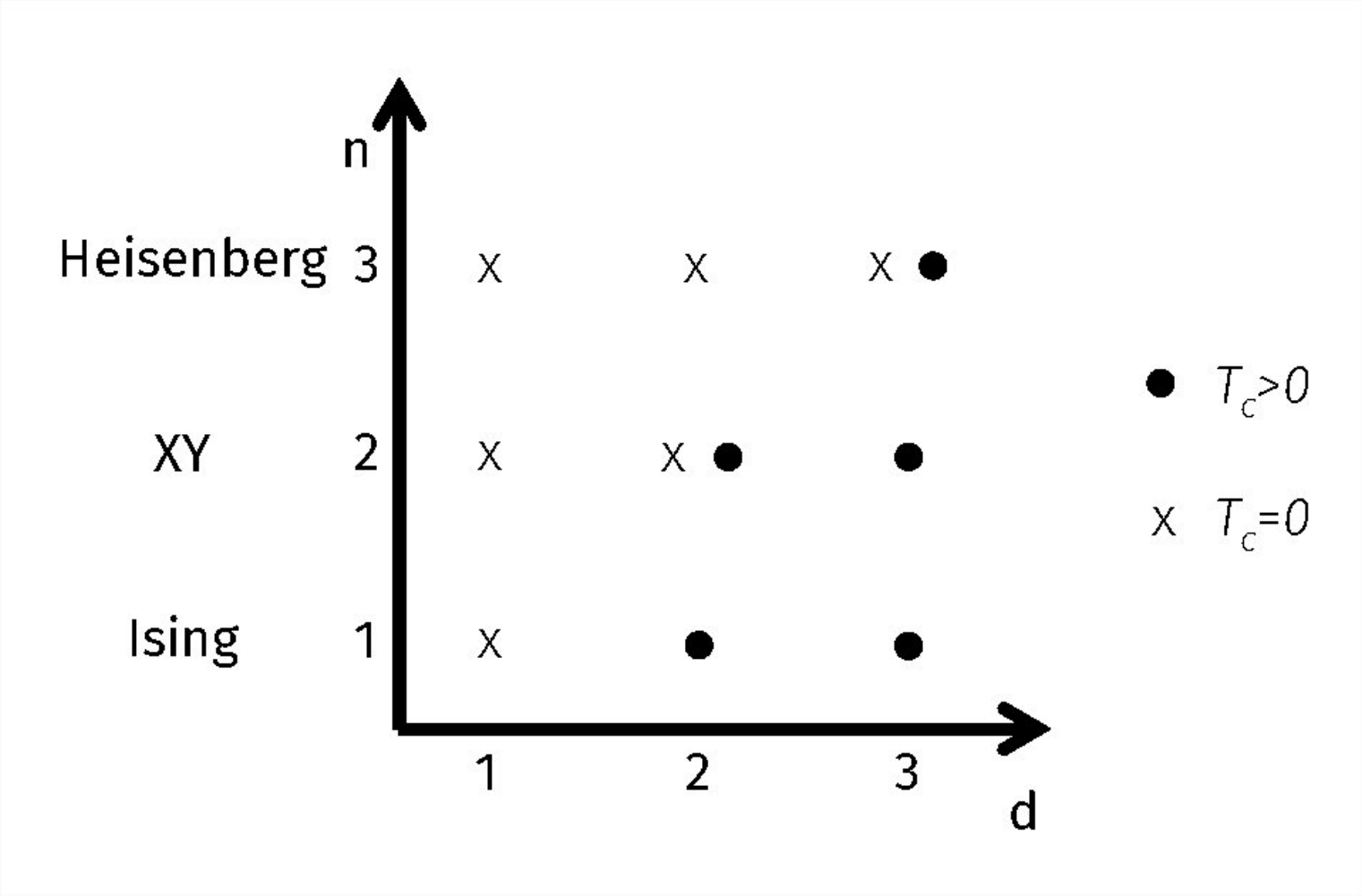

Figure 9: The dependence of the critical temperature on the number of vector components n.